Effect of Na-montmorillonite Clay on the Formation and Dissociation Kinetics of Methane Hydrate

Junjie Ren[1], Mengya Niu[1], Zhenyuan Yin[1*]

1 Institute for Ocean Engineering, Tsinghua Shenzhen International Graduate School, Tsinghua University, Shenzhen 518055, China

ABSTRACT

Silty-clayey host sediments have been widely identified in natural gas hydrate-bearing sediments (HBS). While the effect of clay (montmorillonite, kaolinite, illite, etc.) on the kinetics of CH_4 hydrate formation and dissociation is still not clear. The purpose of this study was to evaluate the kinetics of CH_4 hydrate formation and dissociation in sodium montmorillonite (Na-MMT) suspensions with mass fractions ranging from 0.1 wt% to 9.0 wt%. The results indicate that Na-MMT can promote nucleation but delay the growth kinetics of CH_4 hydrate, as indicated by the shortened induction time and prolonged reaction time. It is worth noting that as the mass fraction increases, the induction time increases while the rate of gas uptake decreases. The morphological analysis was conducted simultaneously. It was discovered that in the presence of montmorillonite, CH_4 hydrate forms initially at the gas-liquid interface and grows upward along the reactor surface. Additionally, the clay-hydrate stratification is evident, indicating that water migrates upward and exacerbates the spatial heterogeneity of CH_4 hydrate. The anti-seepage effect on the clay-water interface prevents water from seeping into the clay layer during the dissociation process. These findings have significant implications for understanding the occurrence of CH_4 hydrate and developing optimized energy recovery strategies in clay-rich sediments.

Keywords: CH_4 hydrate, montmorillonite clay, formation and dissociation kinetics, gas uptake, hydrate-clay morphology

NONMENCLATURE

Abbreviations	
Na-MMT	sodium montmorillonite
SDS	sodium dodecyl sulfate

1. INTRODUCTION

In the deep ocean, natural gas hydrate (NGH) mainly occurs in unconsolidated sands and clay sediments [1, 2]. Clay minerals have an effect on the kinetics of NGH and thus on its occurrence and distribution [3, 4]. In the Shenhu Area of South China Sea (SCS), the gas hydrate deposits are mainly silty clays with clay minerals (26%-30%) such as montmorillonite, illite, kaolinite and chlorite [5]. The small particle size (<5 μm) [6], low permeability (0.001-1.0 mDarcys), large specific surface area (15 - 800 m^2/g), and strong interface reaction activity of clay minerals could potentially affect the kinetic behavior of gas hydrate formation and dissociation. Analysis of SCS mud samples shows that montmorillonite (MMT) is one of the most common clay minerals in NGH bearing sediments [7-10]. The swelling characteristics, the associated reduction in permeability, the negatively-charged surface of MMT are the most significant in several common clays that make MMT the most representative clay [11].

In previous studies, Clennell et al.[12] found that polarized water molecules on clay surfaces inhibit gas hydrate kinetics due to the sufficiently low water activity. Kumar et al.[13] revealed that the presence of bentonite inhibited the growth of hydrate using a stirred tank reactor. While, other studies suggest that the nucleation centers provided by clay surfaces promote MH kinetics [8, 14, 15]. A controversial topic still remains whether the presence of clay in water promotes or inhibits gas hydrate kinetics.

In this study, a series of experiments along with morphology observations was designed to investigate the kinetic characteristics of CH_4 hydrate (MH) in Na-MMT suspensions with varying clay mass fractions (0.1 wt% - 9.0 wt%). An addition of 100 ppm SDS was used in all experimental cases only as a kinetic promoter to prevent the significantly low CH_4 conversion to hydrate.

Besides, the induction time, the gas uptake over time, and the morphology of hydrate in clay suspension were analyzed in detail and compared to elucidate the effect of montmorillonite on the kinetics of MH.

2. EXPERIMENTAL SECTION

2.1 Experimental apparatus and materials

Fig. 1 presents a schematic of the experimental setup. The reactor (V = 156.4 mL) was equipped with two viewing windows. The reactor was wrapped by a cooling jacket in order to adjust the temperature through a circulating chiller. One pressure transducer (±0.01 MPa) and two thermocouples (±0.1 K) were used to obtain P and T. The morphology images were recorded by a CCD camera.

Na-MMT (>98%), CH$_4$ gas (>99.99%) and SDS (Grade AR) were procured. Ultrapure water (18.2 MΩ cm) and Na-MMT suspensions with different mass fractions (0.1 wt% - 9.0 wt%) were prepared. Fig. 2 shows the characteristic information of Na-MMT.

2.2 Experimental procedure

The experimental procedure for the kinetic experiment is as follows: (a) the reactor was cleaned and dried; (b) 60 g suspension was added into the reactor with a constant stirring speed of 300 rpm at T = 288.2 K; (c) residual air was removed and the reactor was pressurized to 8.0 MPa with CH$_4$ gas; (d) cooling the system to T = 275.2 K at a rate of 6.0 K/hr to form MH; (e) MH dissociation was induced by increasing the reactor temperature back to T = 288.2 K at a rate of 6.0 K/hr; (f) a CCD camera was set up to acquire hydrate morphology images and both P and T data were recorded with a frequency of 20s through the processes.

2.3 Calculation method

The calculation method for quantifying the amount of MH during the formation and dissociation processes are based on a volume-balance method [16].

For MH formation, it is described as,

$$CH_4 + N_H H_2 O \rightleftharpoons CH_4 \cdot N_H H_2 O \qquad (1)$$

where N_H = 6.0 is assumed. The volume balance method can be presented as,

$$V_{cell} = V_{G,t} + V_{W,t} + V_{MH,t} + V_{Clay,t}$$
$$= n_{G,t}\rho_{G,t} + n_{W,t}\rho_{W,t} + n_{MH,t}\rho_{G,t} + V_{Clay,t} \qquad (2)$$

where $n_{i,t}$ presents the number of mole at at time t and $\rho_{i,t}$ is the mole volume of the ith phase (i = gas, water, MH) at time t.
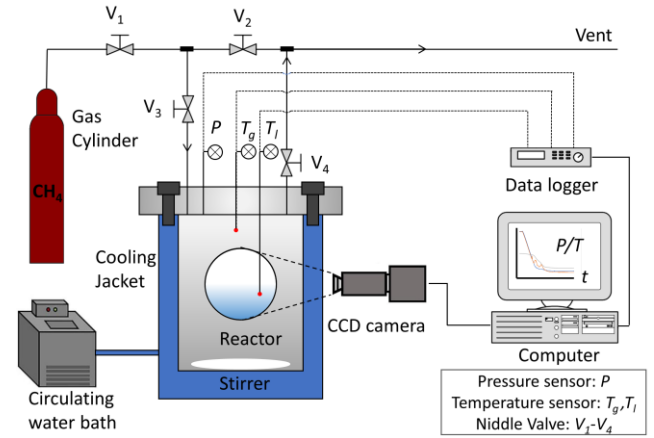
Fig. 1. Schematic of the experimental apparatus.
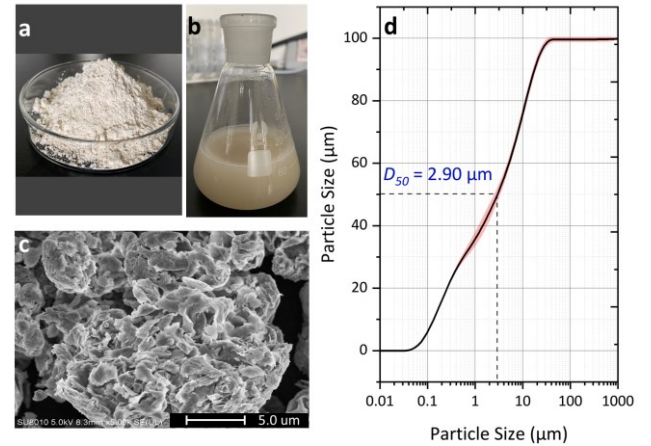
Fig. 2. Pictures of (a) dry Na-MMT clay; (b) 1.0 wt% Na-MMT suspension; (c) SEM image of Na-MMT clay; and (d) particle size distribution of Na-MMT clay.

$$n_{G,t} = n_{G,init}(1 - X_{CH_4,t}) \qquad (3)$$

$$n_{W,t} = n_{W,init}(1 - N_H \times X_{CH_4,t}) \qquad (4)$$

$$n_{MH,t} = n_{G,init} \times X_{CH_4,t} \qquad (5)$$

where $X_{CH4,t}$ represents the conversion of CH$_4$ into MH. The subscript "$init$" refers to the initial condition. The molar volume of H$_2$O and MH is 18.0 cm^3/mol and 136.7 cm^3/mol, respectively [16]. The molar volume of CH$_4$ at time t was estimated using the Peng–Robinson equation of state (PR-EOS) with parameters from Coquelet et al.[17].

3. RESULTS AND DISCUSSION

3.1 Effect of the Na-MMT mass fraction on MH formation kinetics

Na-MMT suspension (5.0wt% and 9.0wt%) were employed with 100ppm SDS added. The induction time (t_{ind}) is estimated based on the time when P-T first enters the MH stable region (the start of supersaturation) to the time that MH particles were identified from visual

observation. Table 1 summarizes t_{ind} in all experimental cases. It was found that t_{ind} decreases with the addition of Na-MMT. However, as the mass fraction of Na-MMT increases, t_{ind} slightly increases and is evidenced by t_{ind} = 76 min in 9.0 wt% Na-MMT suspension.

Fig. 3(a) shows the profiles of gas uptake in the growth stage. In order to quantify the effect of Na-MMT mass fraction on MH growth kinetics, NR_{30} and t_{90} were introduced. It was found that the growth rate of MH reduces with the increasing mass fraction of Na-MMT and is evidenced by the decreasing NR_{30} and increasing t_{90} (62 min in Case-0 < 279 min in Case-5.0 <1649 min in Case-9.0) as shown in Fig. 3(b) and Fig. 3(c).

Table 1 The kinetic parameters in different systems.

Case No.	Suspension composition	t_{ind} (min)	t_{90} (min)	NR_{30} (mol min^{-1} m^{-3})
Case-0	100 ppm SDS	61±28	62±1	42±3
Case-5.0	5.0 wt% Na-MMT + 100 ppm SDS	52±14	279±25	23±6
Case-9.0	9.0 wt% Na-MMT + 100 ppm SDS	76±10	1649±539	8±4

Based on the experimental results, it is concluded that the addition of Na-MMT in H_2O promotes MH nucleation but delays the growth kinetics of MH. One possibility is that the negatively charged clay surface generated a strong electric field which promotes MH nucleation, resulting in a shorter induction time. In terms of growth kinetics, it is speculated that the cations in the suspension restrict the motion of H_2O molecules to construct cage-like clusters toward hydrate formation

[18]. Besides, the clay-bound water reduces the amount of free water for MH formation. The electrostatic interaction between cations and Na-MMT surface is stronger than the van der Waals force between CH_4 and Na-MMT surface, so it is more difficult for CH_4 to enter the interlayer region of Na-MMT for MH formation. Therefore, the retarding effect of Na-MMT on MH growth kinetics increases with increasing mass fraction.

3.2 Effect of the Na-MMT mass fraction on MH dissociation kinetics

As illustrated in Fig. 4(a), dissociation is initially synchronous but deviates in the latter stages. This indicates that the rate of dissociation is more rapid in SDS solution than that in high Na-MMT mass fraction systems (Case-5.0 and Case-9.0). The results were evidenced by the increasing t_{90}' = 152 min in Case-0 < t_{90}' = 180 min in Case-5.0 < t_{90}' = 190 min in Case-9.0 (see Fig. 4b). The results showed that a high mass fraction of clay suspensions necessitated a longer dissociation time. This indicates that Na-MMT has impeded the effectiveness of MH recovery as it would result in greater energy consumption.

3.3 Morphology evaluation of MH formation and dissociation

Fig. 5 presents a comprehensive visual observation of the nucleation, growth and dissociation process of MH in Na-MMT suspensions. t_{ind} was defined as the time when hydrate particles were first observed and t_H was defined as the start of heating.

In SDS solution, MH nucleation occurs initially in the bulk solution at time t_{ind} (see panels a1 and a2). The rapid growth of mushy hydrate above the gas-liquid interface was observed after 10 mins of nucleation and climb up the observation window (see panel a3). Eventually, the
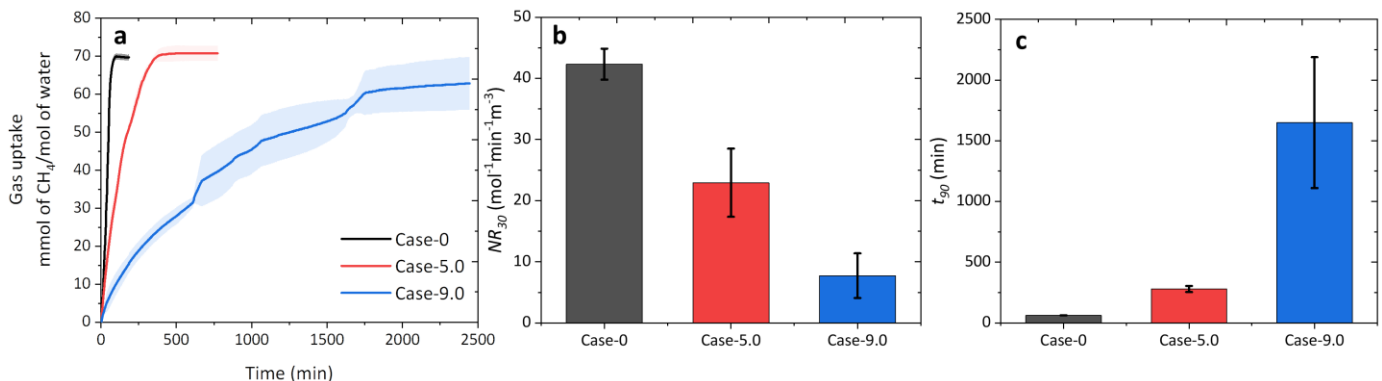
Fig. 3. Kinetics of MH formation characterized by (a) gas uptake; (b) NR_{30}, the normalized rate of hydrate formation; (c) t_{90}, time taken for 90% CH_4 conversion.
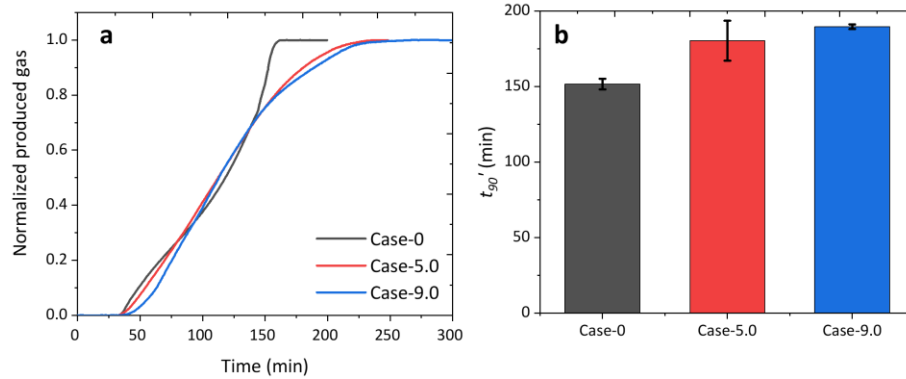
Fig. 4. Kinetics of MH dissociation characterized by (a) Normalized gas production; (b) t_{90}', time taken for 90% CH_4 recovery.

foam-like porous hydrate blocks cover the observation window (see panel a4). Unlike the 100ppm SDS solution, MH nucleation in 5.0 wt% Na-MMT suspension was initially observed at the gas-liquid interface (see panel b1). The upward growth of hydrate film along with the observation window and several hydrate fronts was also observed (see panels b2 and b3). Finally, the opaque MH layer stacks on the observation window gradually (see panel b4). In Case-9.0, a dense MH layer characterized by its dark color and mirror-like appearance forms at the gas-liquid interface resulting in an increase in the mass transfer resistance between the gas and suspension, which is manifested by significant retardation of growth kinetics. It is interesting to note that in the cases of 5.0 wt% and 9.0 wt% Na-MMT suspension, the upward growth habit of MH was significantly reduced and a hydrate-clay stratification was observed. This is evidenced by the morphology images in panels b4 and c4 at the end of the formation process. This can be a partial explanation of the slow kinetics observed earlier, where the contact area between gas and liquid is reduced. In addition, the migration of water upward for hydrate growth was also observed in Fig. 5 panels b3-b4. The formation of MH patches resulted in Na-MMT clay agglomerating in the suspension (see panel b4).

The stirring resumes during the dissociation process, resulting in the rapid decomposition of the hydrate, as evidenced by the presence of a large number of bubbles in the solution, resulting in a non-transparent solution (see panel d2). This is consistent with the phenomenon we observed in Fig. 4a. Additionally, the anti-seepage effect of Na-MMT during the MH dissociation process prevents water from seeping into the clay layer (see panels e1 and e2).

The morphology images in Fig. 5 demonstrate that the presence of Na-MMT retards the growth of MH in clay suspension, resulting in a relatively dense layer of MH rather than the porous hydrate seen in the SDS solution. The dense MH layer reduces the contact area and increases the mass transfer resistance for MH formation. In addition, the agglomeration of clay particles locks free water for MH formation. The preceding provides possible explanations for the slow gas uptake profiles observed in clay-rich suspension.

3.4 Implication on NGH occurrence and energy recovery

As discussed above, we found that the presence of clay can promote the nucleation of MH, delay the kinetics of MH growth and dissociation and lead to a hydrate-clay stratification and anti-seepage effect. For NGH occurrence, the presence of Na-MMT facilitates NGH form and likely results in a hydrate-clay layered regime. For energy recovery, the anti-seepage effect of clay is pronounced, implying that excessive local water production may occur in the actual clay-rich layer.

CONCLUSION

The following conclusions can be drawn from this study:
a. Na-MMT facilitates the nucleation of MH, and an increased mass fraction of Na-MMT results in a prolonged t_{ind}.
b. Na-MMT delays the growth and dissociation kinetics of MH. Increased clay content is associated with a lower rate of gas uptake (1/6 fold NR_{30}) and a longer dissociation time.
c. The effect of Na-MMT on the kinetics of MH, the hydrate-clay stratification and anti-seepage effect offer explanation on the hydrate occurrence in clay-silty hydrate-bearing sediments and have implications on the energy recovery process from these types of hydrate reservoirs.

4
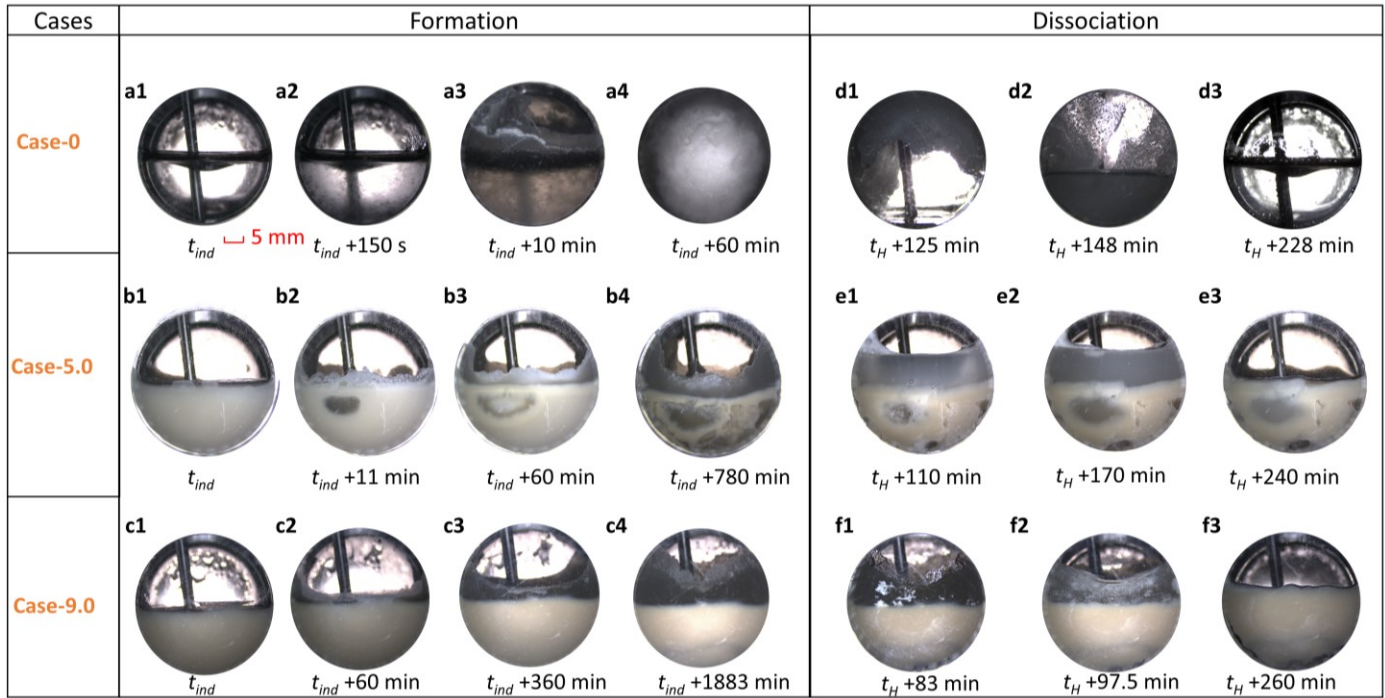
Fig. 5. Morphology of MH formation and dissociation in Na-MMT suspensions (100 ppm SDS) with varying mass fractions.

REFERENCE

[1] Cygan RT, Guggenheim S, Koster van Groos AF. Molecular models for the intercalation of methane hydrate complexes in montmorillonite clay. J Phys Chem B. 2004;108:15141-9.

[2] Yeon S-H, Seol J, Seo Y-j, Park Y, Koh D-Y, Park K-P, et al. Effect of interlayer ions on methane hydrate formation in clay sediments. J Phys Chem B. 2009;113:1245-8.

[3] Van Groos AK, Guggenheim S. The stability of methane hydrate intercalates of montmorillonite and nontronite: Implications for carbon storage in ocean-floor environments. Am. Mineral. 2009;94:372-9.

[4] Schroeder A, Wiesner MG, Liu Z. Fluxes of clay minerals in the South China Sea. Earth Planet. Sci. Lett. 2015;430:30-42.

[5] Li J-f, Ye J-l, Qin X-w, Qiu H-j, Wu N-y, Lu H-l, et al. The first offshore natural gas hydrate production test in South China Sea. China Geology. 2018;1:5-16.

[6] Hubert F, Caner L, Meunier A, Ferrage E. Unraveling complex< 2 µm clay mineralogy from soils using X-ray diffraction profile modeling on particle-size sub-fractions: Implications for soil pedogenesis and reactivity. Am. Mineral. 2012;97:384-98.

[7] Martín-Puertas C, Mata M, Fernández-Puga M, del Río VD, Vázquez J, Somoza L. A comparative mineralogical study of gas-related sediments of the Gulf of Cádiz. GEO-MAR LETT. 2007;27:223-35.

[8] Cha S, Ouar H, Wildeman T, Sloan E. A third-surface effect on hydrate formation. J. Phys. Chem. C. 1988;92:6492-4.

[9] Clennell MB, Hovland M, Booth JS, Henry P, Winters WJ. Formation of natural gas hydrates in marine sediments. Ann. N. Y. Acad. Sci. 1999;912:887-96.

[10] Li Y, Chen M, Song H, Yuan P, Zhang B, Liu D, et al. Effect of cations (Na+, K+, and Ca2+) on methane hydrate formation on the external surface of montmorillonite: insights from molecular dynamics simulation. ACS Earth Space Chem. 2020;4:572-82.

[11] Wu Z, Li Y, Sun X, Wu P, Zheng J. Experimental study on the effect of methane hydrate decomposition on gas phase permeability of clayey sediments. Appl. Energy. 2018;230:1304-10.

[12] Clennell MB, Hovland M, Booth JS, Henry P, Winters WJ. Formation of natural gas hydrates in marine sediments: 1. Conceptual model of gas hydrate growth conditioned by host sediment properties. J. Geophys. Res. Sol. Ea. 1999;104:22985-3003.

[13] Kumar A, Sakpal T, Roy S, Kumar R. Methane hydrate formation in a test sediment of sand and clay at various levels of water saturation. Can J Chem. 2015;93:874-81.

[14] Park T, Kwon T-H. Effect of electric field on gas hydrate nucleation kinetics: Evidence for the enhanced kinetics of hydrate nucleation by negatively charged clay surfaces. Environ. Sci. Technol. 2018;52:3267-74.

[15] Lamorena RB, Lee W. Formation of carbon dioxide hydrate in soil and soil mineral suspensions with electrolytes. Environ. Sci. Technol. 2008;42:2753-9.

[16] Yin Z, Wan Q-C, Gao Q, Linga P. Effect of pressure drawdown rate on the fluid production behaviour from methane hydrate-bearing sediments. Appl. Energy. 2020;271:115195.

[17] Coquelet C, Chapoy A, Richon D. Development of a new alpha function for the Peng–Robinson equation of state: comparative study of alpha function models for pure gases (natural gas components) and water-gas systems. Int. J. Thermophys. 2004;25:133-58.

[18] Yi L, Liang D, Zhou X, Li D, Wang J. Molecular dynamics simulations of carbon dioxide hydrate growth in electrolyte solutions of NaCl and MgCl2. Mol. Phys. 2014;112:3127-37.